Multi-wavelets P-Impedance for the Brazilian Pre-Salt Reservoirs Characterization: An Example in the Santos Basin

Talles Meneguim*, Yves dos Reis Assis, Ariely Luparelli Rigueti, Renata Giacomel, Alexandre Maul, Filipe Borges
(Petrobras S.A.)

Abstract

The pre-salt province of Santos Basin, Brazilian offshore, has pushed an increase in the E&P activities due to the presence of large hydrocarbon accumulations. In general, these carbonatic reservoirs are covered by a complex salt section, which varies in thickness from a few meters to over 3 km. This salt section displays complex features such as salt walls, canopies, and welds. Above the salt section lies a thick siliciclastic Albian wedge, which poses challenges for seismic amplitude response. Therefore, due to the salt section and Albian wedge, the reservoir's seismic response is affected by shadow zones and frequency loss. Besides, when a seismic inversion is performed considering a thick or variating thickness seismic section, the estimation of a single global wavelet arises uncertainty for the inversion process. In this work, we propose a methodology to obtain a seismically inverted 3D P-impedance using variable wavelets estimated from wells. The inverted P-impedance calculated with our methodology incorporates the non-homogeneous seismic energy arriving at the reservoir level, matching both well and seismic data better than that obtained using just one global wavelet in the seismic inversion.

Introduction

Seismic data plays a crucial role in oil and gas field development projects through qualitative and quantitative seismic interpretation, facies modeling, geomechanical studies, and uncertainty analysis (Meneguim *et al.*, 2015; Meneguim *et al*., 2016). However, seismic amplitudes at depths exceeding 5000m (Figure 1) can be degraded in several ways.

Imaging problems caused by uneven illumination can create shadow zones due to the significant variation in salt thickness and the presence of a siliciclastic Albian wedge (Maul *et al.*, 2015, Camargo *et al.*, 2022).

Although halite is the most common salt present, there are also other evaporites such as anhydrite, tachyhydrite, and carnallite (Yamamoto *et al.*, 2016). Additionally, the frequency bandwidth can be affected by the loss of low frequencies during seismic acquisition (source and receiver ghosts) and by the loss of high frequencies due to absorption (siliciclastic Albian wedge and salt layer). The drilled wells in the study area in Figure 1 are mounds with similar elastic properties and geologic facies. The seismic energy variation from the leftmost well to the rightmost wells shows the impact of uneven reservoir illumination and loss of frequency bandwidth since the contrast of reservoir properties is similar in the wells.

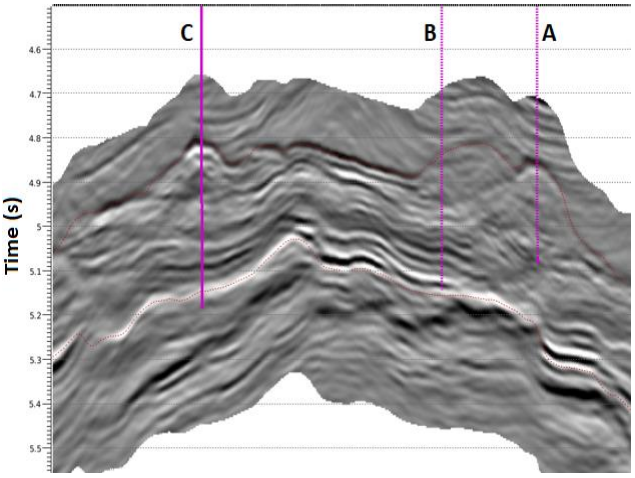

***FIG 1**: Pre-Salt migrated seismic amplitude in a full-stack reservoir section. This figure illustrates the significant variation in seismic energy at the leftmost well, when compared to the two rightmost wells. The distance between wells B and A is about 1.5 km.*

Once the reservoir seismic response is affected by shadow zones and loss of frequency due to the Salt section and Albian wedge the main objective of this article is to show for a highly non-homogeneous seismic energy pre-salt reservoir that a multi-wavelets 3D P-Impedance is a powerful approach to better estimate the P-Impedance into the study case as well as to recover some weakened geological events in the input seismic data.

To mitigate these issues, a customized multi-wavelets P-Impedance estimative in the study area is mandatory. The multi-wavelets P-Impedance approach considers areal variations of seismic energy in the well's positions to estimate more representative wavelets, rather than using only one global wavelet for the whole area. Careful execution of this process is shown to reduce errors in the estimation of 3D P-impedance and, consequently, in several reservoir characterization workflows like porosity prediction, facies modelling, fluid saturation, and elasticity modulus estimation (Grana et al., 2021).

Methodology

The seismic inversion processes use reflection seismic data to estimate P-impedance, enabling quantitative estimation of rock properties. A common inversion method such as Constrained Sparse-spike Inversion (CSSI) was used in this work. It involves the straightforward convolution of a reflectivity model with an estimated wavelet to produce synthetic traces, which are then compared to the input seismic traces, and the reflectivity model is updated to ensure careful matching between the synthetic and seismic data, as well as lateral/vertical smoothness and sparsity in the P-impedance.

For this study, we selected nine wells drilled in a pre-salt portion of the Santos Basin. Seismic-to-well ties were used to obtain nine wavelets, one per well (Figure 2, left side). The wellbore P-impedance for these wells has a similar range of variation, so the main difference between wavelets is related to imaging problems in the seismic data. To illustrate the variation in seismic energy within the reservoir: the highest amplitude wavelet is three times that of the lowest amplitude wavelet, and the frequency range varies by a factor of two from the highest to lowest frequency wavelet.

Given this variation in wavelets, they were reorganized into three groups based on amplitude: low, medium, and high. Each group represents the average of wavelets from three wells. Figure 2 (right side) shows these three groups of basis wavelets.

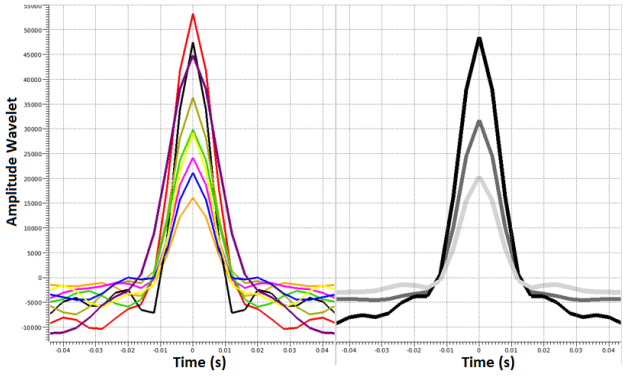

***FIG 2**: Left: Wavelets extracted from nine wells. Right: their reorganization into three amplitude groups (side).*

Three deterministic acoustic CSSI were performed to obtain the reservoir P-impedance, each corresponding to one of the three basis wavelets shown on the right side of Figure 2. The inversion parameterization, low-frequency P-impedance initial model, and input seismic data were the same for all three inversion processes. These three inverted P-impedances form our basis P-impedances derived from the basis wavelets.

The multi-wavelets P-impedance is a linear combination of the basis P-impedances, with three appropriate weights for every spatial coordinate (x,y). The weights for each of the inverted P-impedances should approach 1 as we approach a well whose wavelet was used to perform that inversion. Another constraint is that the sum of these three weights must equal one for every point.

The best results for the multi-wavelets P-impedance were obtained using normalized inverse square distance weighting with local "poles" at the well positions. From this multi-wavelets P-impedance, a multi-wavelet P-reflectivity was also computed for zero-offset R_{p0}. In addition to improvements in the multi-wavelet P-impedance itself, improvements were also observed in the synthetic seismic data derived from the multi-wavelet P-reflectivity.

Results

The results were analyzed both qualitatively, through drilled well sections, and quantitatively, using cross-plots. Figures 3 and 4 show two full-band multi-wavelets P-impedance sections with the corresponding P-impedance well logs.

In Figure 3, the left side shows the result of a seismic inversion using one average global wavelet, while the right side shows the multi-wavelet P-impedance. Well A requires the lower amplitude wavelet from the wavelet group, while well B requires the higher amplitude wavelet. The distance between these wells is 1.5 km. On the left side, the average global wavelet did not match the circled events. In contrast, on the right side, these events are much better represented due to the application of the multi-wavelets approach.

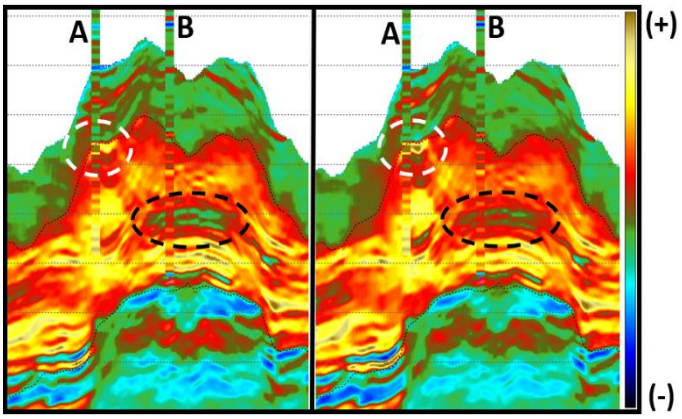

***FIG 3:** Comparison of inverted P-impedance using an average global wavelet (left side) and multi-wavelets P-impedance (right side). A and B represent drilled wells, with their corresponding P-impedance logs. Observe the enhanced match between P-Impedance well logs and multi-wavelets P-Impedance on the right side compared to the left side in the circled events.*

Figure 4 shows another comparison of inverted P-impedance using the average global wavelet (upper side) and multi-wavelet P-impedance (lower side). Well C requires the lower amplitude wavelet from the wavelet group, while well D requires the higher amplitude wavelet. The distance between these wells is circa 5 km. On the upper panel, the average global wavelet did not adjust the appointed events. In contrast, on the lower panel, these events are much better represented, due to the application of the multi-wavelets approach.

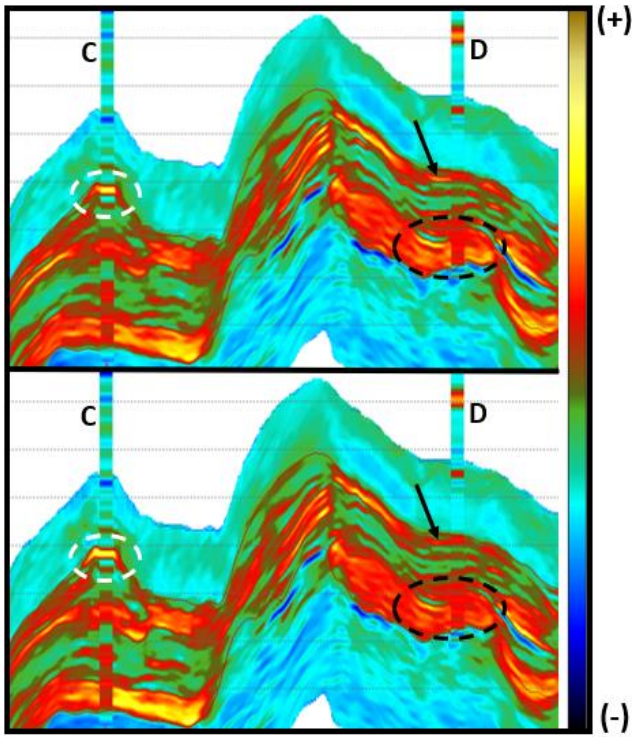

FIG 4: *Comparison of inverted P-impedance using one average global wavelet (upper panel) and multi-wavelets P-impedance (lower panel). C and D represent drilled wells, with their corresponding P-impedance logs. Observe the enhanced match between P-Impedance well logs and multi-wavelets P-Impedance in the lower side compared to the upper side in the circled events.*

Because the multi-wavelet P-impedance cube delivered improved qualitative results, it was used to compute a multi-wavelet zero-offset P-reflectivity R_{p0}. This reflectivity was used to generate a synthetic seismic data, by the application of a bandpass filter to match the frequency bandwidth of the field raw seismic data.

Figures 5 and 6 show a comparison of field seismic data (upper panels) and multi-wavelets reflectivity, filtered at the same frequency bandwidth as the field data (lower panels). The dashed ellipses highlight regions where, on the upper panels (field data), several seismic events are poorly imaged, appearing as vanished and/or “blurred” reflectors.

However, after applying the multi-wavelets approach to compensate for non-homogeneous illumination within the reservoir, these seismic events become more prominent (lower panels). This results in a significant spectral frequency enhancement, great for seismic reservoir characterization, especially when dealing with thin layers/features.

A quantitative analysis of the multi-wavelets approach was also performed. Figure 7 analyzes the P-impedance within the seismic frequency bandwidth, referred to as band-pass P-impedance (BP-IP), for both the seismically inverted BP-IP using one average global wavelet and the multi-wavelets (BP-IP) modeled cube. Ideally, at well positions, a zero-error P-impedance cube should deliver a 1:1 ratio with the well’s BP-IP. In the upper plot of Figure 7, well BP-IP is plotted on the x-axis and BP-IP from the average global wavelet is plotted on the y-axis. The best linear fit passing through the origin (red line) has an angular slope of 0.58, which is far from the desired 1:1 relation (black line). On the lower plot of Figure 7, well BP-IP remains on the x-axis, while the y-axis now represents BP-IP from the multi-wavelets approach. The best linear fit passing through the origin (red line) has an angular slope of 0.72, which is much closer to the desired 1:1 relation (black line). The multi-wavelets approach to P-Impedance inversion reduced the maladjustment in the angular slope by 66%, compared to using a global average wavelet (Figure 7).

Figure 8 compares the frequency spectrum of field data (black line) and multi-wavelets P-reflectivity R_{p0} (green line), filtered at the seismic bandwidth. The field data shows a central peak followed by a sharp decline in frequency, while the multi-wavelet R_{p0} has a broader, flatter spectrum. This is consistent with Figures 5 and 6, where poorly imaged events are more noticeable in the multi-wavelet R_{p0}. The amount of seismic energy recovered by the multi-wavelet reflectivity, represented by the area under the curve in Figure 8, was 52% greater than that of the raw seismic data.

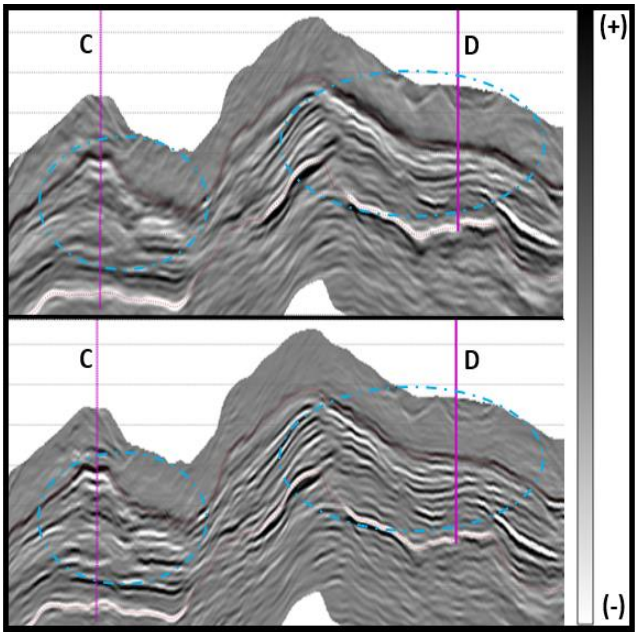

FIG 5: *Comparison of field seismic data (upper panel) and multi-wavelets P-reflectivity R_{p0} filtered to the same bandwidth of the seismic data (lower panel). Dashed ellipses indicate seismic events that are vanished or blurred on the upper image and that are more prominent on the lower one. This comparison allows us to confirm the quality results obtained through the multi-wavelets approach here presented. C and D represent drilled wells.*

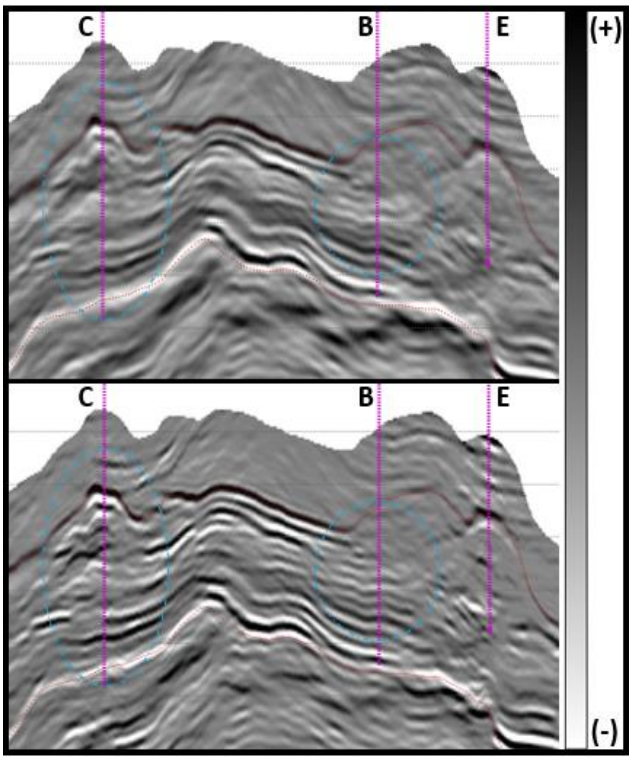

FIG 6: *Comparison of field seismic data (upper panel) and multi-wavelets P-reflectivity R_{p0} filtered to the same bandwidth of the seismic data (lower panel). Once again, dashed ellipses indicate seismic events that are vanished or blurred on the upper image and that are more prominent and apparent on the lower one, still confirming the goals we had proposed by this methodology. B, C, and E represent drilled wells.*

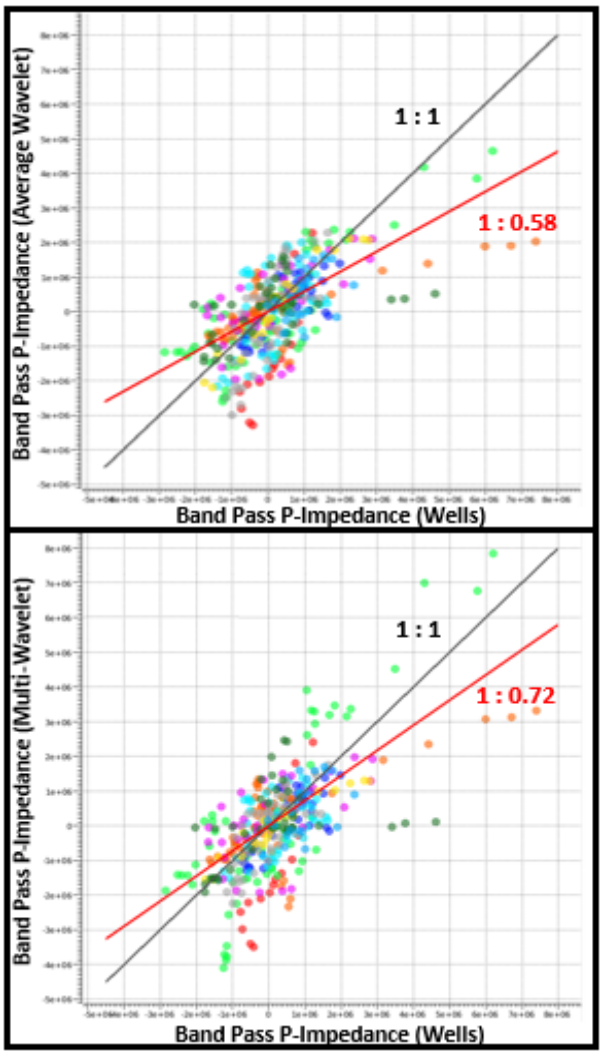

FIG 7*: Comparison of band-pass P-Impedance from seismic inversion using global average wavelet (angular slope: 0.58) and multi-wavelets approach (angular slope: 0.72) with well log data. The desired angular slope is 1 (black line). This comparison allows us to confirm the improvement in the P-Impedance obtained through the multi-wavelets approach. Points are colored by the 10 drilled wells in the area.*

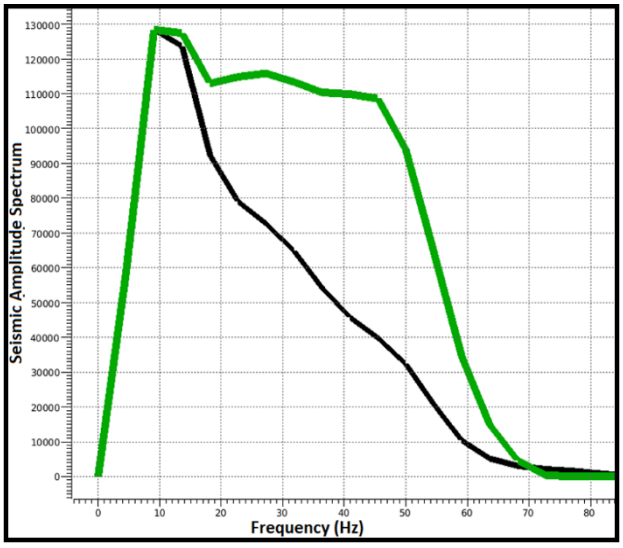

FIG 8: *Comparison of frequency spectrum between field data (black line) and multi-wavelets P-reflectivity R_{p0} (green line), filtered at seismic bandwidth. The multi-wavelets R_{p0} recovers energy from frequency components that are weakened in the raw seismic data indicating one more important advantage of the multi-wavelet's approach here presented.*

Conclusions

The multi-wavelets approach in constructing a 3D P-Impedance cube accounts for non-homogeneous seismic illumination in each well's neighborhood and it was mandatory for the complex pre-salt reservoir study case in the Santos Basin. This approach showed qualitative improvements in the well's sections in matching the wells-log P-Impedance when compared to using a global average wavelet.

Multi-wavelets P-reflectivity R_{p0}, filtered to the seismic bandwidth, showed qualitative improvements, with more noticeable seismic events compared to field raw data. Quantitative improvements were observed in the angular slope of the cross-plot between estimated and well-log band-pass P-Impedances. The multi-wavelets R_{p0}frequency spectrum also showed a 52% increase in recovered harmonic frequency energy compared to raw seismic data. The qualitative and quantitative analyses suggest that a multi-wavelets P-Impedance is more reliable for modeling porosity, geological facies, and elastic properties. Multi-wavelets P-reflectivity R_{p0} can support stratigraphic seismic interpretation, by revealing vanished and blurred events that are challenging to identify in the filed data.

Acknowledgments

The authors would like to thank Petrobras for the financial support and time dedication to develop this work, as well as for the permission to publish it.

References

Camargo, G.N., González, M., Borges, F., Maul, A. & Mohriak, W.U. 2022. Challenges for seismic velocity m of rafts and impacts for pre-salt depth estimations. Petroleum Geosciences, 29.

Grana, D., Tapan M. & Doyen P. 2021. Seismic Reservoir Modeling: Theory, Examples, and Algorithms.

Maul, A., Jardim, F., Falcão, L. & González, G. 2015. Observing amplitude uncertainties for a pre-salt reservoir using illumination study (hit-maps). 77th EAGE Conference and Exhibition, Madrid, Spain.

Meneguim, T.B., Mendes, S.C., Maul, A.R., Falcão, L., González, M.G. & González G. 2015. Combining seismic facies analysis and well Information to guide new interval velocity models for a pre-salt study, Santos Basin, Brazil. In: 14th International Congress of the Brazilian Geophysical Society & Expogef, Rio de Janeiro, RJ, Brazil.

Meneguim, T.B., Pereira, C.E.L., Almeida Jr, M.P., Born, E., Proença, T. & Gomez, L., 2016, Effects of Post Stack Seismic Data Conditioning on Impedance Inversion for Reservoir, Santos Basin, Brazilian Pre-Salt. 78th. EAGE Conference and Exhibition 2016, Madrid, Spain.

Yamamoto, T., Maul, A., Born, E., Gobatto, F., Relvas, M.T & González, M. 2016. Incorporação de estratificações salíferas na modelagem de velocidade de uma jazida da Bacia de Santos. VII Simpósio Brasileiro de Geofísica, Ouro Preto, Brazil.